

Molecular-level origin of the carboxylate head group response to divalent metal ion complexation at the air-water interface

Joanna K. Denton^a, Patrick J. Kelleher^a, Mark A. Johnson^{a,1}, Marcel D. Baer^b, Shawn M. Kathmann^b, Christopher J. Mundy^{b,c}, Bethany A. Wellen Rudd^{d,e}, Heather C. Allen^d, Tae Hoon Choi^f, and Kenneth D. Jordan^{f,g}

^aSterling Chemistry Laboratory, Yale University, New Haven, CT 06520; ^bPhysical Sciences Division, Pacific Northwest National Laboratory, Richland, WA 99352; ^cDepartment of Chemical Engineering, University of Washington, Seattle, WA 98195; ^dDepartment of Chemistry & Biochemistry, The Ohio State University, Columbus, OH 43210; ^eDepartment of Chemistry, Ohio Wesleyan University, Delaware, OH 43015; ^fDepartment of Chemistry, University of Pittsburgh, PA 15260; and ^gDepartment of Chemical and Petroleum Engineering, University of Pittsburgh, Pittsburgh, PA 15260

Contributed by Mark A. Johnson, May 31, 2019 (sent for review November 7, 2018; reviewed by Paul S. Cremer and Joseph S. Francisco)

We exploit gas-phase cluster ion techniques to provide insight into the local interactions underlying divalent metal ion-driven changes in the spectra of carboxylic acids at the air-water interface. This information clarifies the experimental findings that the CO stretching bands of long-chain acids appear at very similar energies when the head group is deprotonated by high subphase pH or exposed to relatively high concentrations of Ca2+ metal ions. To this end, we report the evolution of the vibrational spectra of size-selected $[Ca^{2+} \cdot RCO_2^{-}]^{+} \cdot (H_2O)_{n=0 \text{ to } 12}$ and $RCO_2^{-} \cdot (H_2O)_{n=0 \text{ to } 14}$ cluster ions toward the features observed at the air-water interface. Surprisingly, not only does stepwise hydration of the RCO2 anion and the [Ca2+·RCO2-]+ contact ion pair yield solvatochromic responses in opposite directions, but in both cases, the responses of the 2 (symmetric and asymmetric stretching) CO bands to hydration are opposite to each other. The result is that both CO bands evolve toward their interfacial asymptotes from opposite directions. Simulations of the [Ca2+·RCO2-]+·(H2O)n clusters indicate that the metal ion remains directly bound to the head group in a contact ion pair motif as the asymmetric CO stretch converges at the interfacial value by n = 12. This establishes that direct metal complexation or deprotonation can account for the interfacial behavior. We discuss these effects in the context of a model that invokes the water network-dependent local electric field along the C-C bond that connects the head group to the hydrocarbon tail as the key microscopic parameter that is correlated with the observed trends.

interface | spectroscopy | infrared | surfactant | metal complex

he local environments of the ionic head groups of surfactant molecules at the air-water interface are of critical importance in understanding the physical processes responsible for the transfer of organic carbon and transition metal ions into the atmosphere (1–4). Here, we are concerned with the nature of the species formed when fatty acids at the interface are deprotonated by the presence of Ca²⁺ ions in the bulk (subphase) solution. The methods of choice for extracting this molecular-level information are variations on interfacial vibrational spectroscopy, such as second harmonic generation (5–8), sum-frequency generation (SFG) (9-18), and infrared reflection-absorption spectroscopy (IRRAS) (19-22). In the case of fatty acids, the CO stretching modes (carbon oxygen stretches of the RCO₂⁻ anion) provide natural vibrational reporters for the local environment of the head group. Fig. 1 contrasts the effect on carboxylic acids of the presence of 0.3 M Ca²⁺ metal ions in the subphase (Fig. 1C) with that due to simple acid deprotonation at high subphase pD (10.5 in Fig. 1B) caused by the addition of NaOD. On increasing the pH or adding CaCl₂ to the subphase, the 2 widely split CO bands (ν^{C-OH} and $\nu^{C=O}$) in the neutral acid spectrum (Fig. 1A) are replaced by 2 features at \sim 1,413 and \sim 1,551 cm⁻¹. nominally assigned to the symmetric (ν_s^{COO}) and asymmetric (ν_{qq}^{COO}) stretching fundamentals arising from the deprotonated carboxylate group. This observation is consistent with previous work on related systems as summarized in SI Appendix, Table S1. A curious aspect of these results is that, although the dominant feature in the Ca^{2+} spectrum is clearly broader than that obtained at pD = 10.5, it is evident that both schemes yield very similar bands, raising the question of whether Ca^{2+} promotes deprotonation of the acid at relatively low pH or is complexed directly to the anionic head group in a contact ion pair.

Several studies have considered the M²⁺-induced spectral response of carboxylates in various chemical environments (19, 23–30). In anhydrous crystals, for example, where the binding configuration can be established by crystallography, a correlation was found between the binding motif and the splitting between the carboxylate stretching modes (25, 31). In aqueous environments, the binding configuration of the system under study is less clear and raises a scenario where acetate solutions of Ca²⁺ and Mg²⁺ are "ionic" in the sense that the acetate groups do not penetrate the inner hydration spheres of either cation (23, 24).

Significance

The transport of divalent metal ions (e.g., Mg²⁺ and Ca²⁺) into the troposphere is thought to arise from preferential complexation with anionic head groups of fatty acids at sea-spray aerosol surfaces. Attempts to quantify the formation of these complexes by monitoring the vibrational frequencies of the CO stretching vibrations have proven to be inconclusive, however, because the metal ion-driven spectral response is surprisingly similar to that displayed by the fully hydrated anion. We trace the origin of these spectral responses by measuring the stepwise hydration behaviors of both the carboxylate head group and the contact ion pair. These trends reveal the critical contribution of chain deformation to the structural interpretation of surface-sensitive spectral signatures of ion complexation at the interface.

Author contributions: M.A.J. designed research; J.K.D., P.J.K., M.D.B., S.M.K., C.J.M., B.A.W.R., T.C., and K.D.J. performed research; M.D.B., S.M.K., C.J.M., B.A.W.R., H.C.A., T.C., and K.D.J. contributed new reagents/analytic tools; J.K.D., P.J.K., M.A.J., M.D.B., S.M.K., C.J.M., B.A.W.R., H.C.A., T.C., and K.D.J. analyzed data; and J.K.D., P.J.K., and M.A.J. wrote the paper.

Reviewers: P.S.C., Pennsylvania State University; and J.S.F., University of Pennsylvania.

The authors declare no conflict of interest.

Published under the PNAS license

Data deposition: The data used to generate the figures and conclusions in this paper are included in a dataset hosted by the University of California, San Diego Library Digital Collections as part of the Center for Aerosol Impacts on Chemistry of the Environment (CAICE) Collection (https://doi.org/10.6075/J0GH9G3H).

¹To whom correspondence may be addressed. Email: mark.johnson@yale.edu.

This article contains supporting information online at www.pnas.org/lookup/suppl/doi:10.1073/pnas.1818600116/-/DCSupplemental.

Published online July 5, 2019

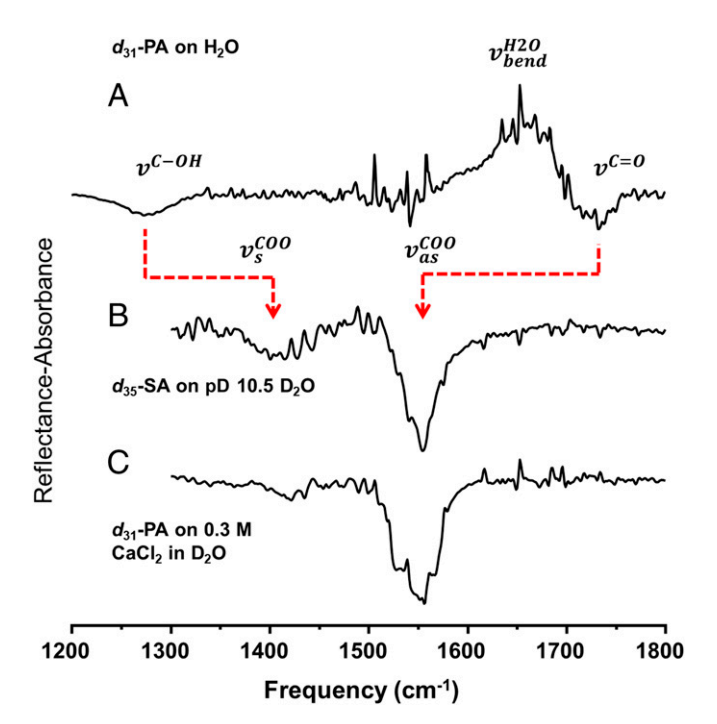


Fig. 1. IRRAS spectra of monolayers (20.5 Ų per molecule) of (A) d₃₁-PA on neat H₂O, (B) d₃₅-SA on D₂O with a subphase pD of 10.5, and (C) d₃₁-PA on D₂O with a subphase CaCl₂ concentration of 0.3 M. Features assigned to the 2 carbon–oxygen stretching modes of the intact carboxylic acid are developed ν^{C-OH} and ν^{C-OH} and ν^{C-O} in A along with the water bending mode ($\nu^{H_2O}_{bend}$). Peaks assigned to the symmetric and asymmetric stretching modes of the deprotonated carboxylate head group are denoted ν^{COO}_s and ν^{COO}_{as} , respectively, in B. Note that, with the exception of the H₂O bend, peaks appear as negative bands due to the experimental geometry.

At the air–water interface, the presence of subphase metal ions $(Ca^{2+}$ and $Mg^{2+})$ has been observed to alter the experimentally determined pH dependence of the ionized fraction of fatty acids (19, 32). This has been interpreted to indicate formation of contact ion pairs based on the comparison of observed behavior with predictions based on the purely electrostatic Gouy–Chapman formalism, which predicts the deprotonation fraction in the absence of complexation (19, 33). The close proximity of the ν_{as}^{COO} band measured here by IRRAS for the hydrated carboxylate head group (Fig. 1 B, 1,553 cm⁻¹) and that purported to occur as the Ca^{2+} contact ion pair (Fig. 1 C, 1,549 cm⁻¹), therefore, raises the question of how the 2 seemingly disparate processes—simple pH-induced deprotonation vs. direct Ca^{2+} metal ion complexation—can give rise to nearly identical CO stretching bands.

Here, we clarify the factors that control the response of the CO stretching fundamentals of the carboxylate head group to hydration and ion complexation. We accomplish this by following the evolution of these bands starting from the isolated gas-phase carboxylate ion (CD₃CD₂CO₂⁻; hereafter denoted d-OPr⁻) (Fig. 24) and the cationic binary ion pair $(d-[Ca^{2+}OPr^{-}]^{+})$ (Fig. 2B) with stepwise addition of water molecules. These solvation trends are followed to cluster sizes that are sufficiently large to recover the observed interfacial behavior. The resulting data are available at refs. 34 and 35. The calculated microhydration structures for d-OPr $^-$ (H₂O)₅ and d-[Ca $^{2+}$ ·OPr $^-$] $^+$ ·(H₂O)₅ are compared in Fig. 2 C and D to illustrate the enhancement of the interwater hydrogen bonding network in the hydrated anion. The perdeuterated isotopologues were used to avoid complications in the C-O stretching region caused by nearby levels involving C-H modes (12, 27, 36-38). The spectral trends are interpreted with theoretical methods appropriate for the size regime to reveal the

microscopic mechanics that underlie the spectroscopic response of carboxylate head groups to their local environments.

This work follows a recent gas-phase spectroscopic study by DePalma et al. (36), which isolated the intrinsic vibrational signatures of the contact ions pairs $[M^{2+} \cdot RCO_2^{-}]^+$ with (M = Mg,Ca; $R = -CD_3$, $-CD_2CD_3$). The isolated contact ion pairs occur with a bidentate motif in which the metal ions reside between the oxygen atoms in the arrangement depicted in Fig. 2B (for Ca^{2+}). An important aspect of that study is that the nominal ν_s^{COO} mode was found to be strongly coupled to the C-C stretching motion of the bond connecting the head group to the alkyl chain in the metal complexes, consistent with observations by other investigators (27, 37, 39). This implies that the splitting between the peaks traditionally assigned to ν_s^{COO} and ν_{as}^{COO} stretches may not simply reflect the coupling between the 2 CO oscillators (27). In keeping with traditional notation, however, we refer to the mixed levels as ν_s^{COO} hereafter in this work. The earlier cluster ion study (36) focused on the d-OPr anion to provide a sufficiently long chain length to capture this mixing effect and followed the hydration behavior for the small water clusters d-[Mg²⁺·OPr⁻]⁺·(H₂O)_{n=1 to 4}. The spectra of several $RCO_2^-[R = H, -CH_3, -CD_2CD_3, -(CH_2)_{10}CH_3]$ complexes are compared in SI Appendix, Fig. S1 to illustrate the negligible chain length dependence on the character of the CO bands for R larger than -CD₂CD₃. Interestingly, the strongly redshifted ν_{as}^{COO} band in the bare $[Mg^{2+} \cdot OPr^{-}]^{+}$ contact ion pair (relative to bare d-OPr⁻) was shown to exhibit an unusual solventinduced blue shift, raising the question of how these cluster bands evolve toward the band positions in the interface. Here, we extend this study to the more important Ca²⁺ contact ion pair as well as to larger hydrates and complement these results with spectroscopic measurements on the d- $\overline{OPr}^-(H_2O)_{n=1 \text{ to } 14}$ clusters. To make the connection to the interfacial spectroscopic response, we carried out measurements of fatty acids at the air-water interface using IRRAS, because it preferentially yields information about the most responsive ν_{α}^{COO} transitions owing to the transition moments at play in this system. We note that, because IRRAS is not a surfacespecific method (as opposed to SFG), the long-chain d₃₅-stearic

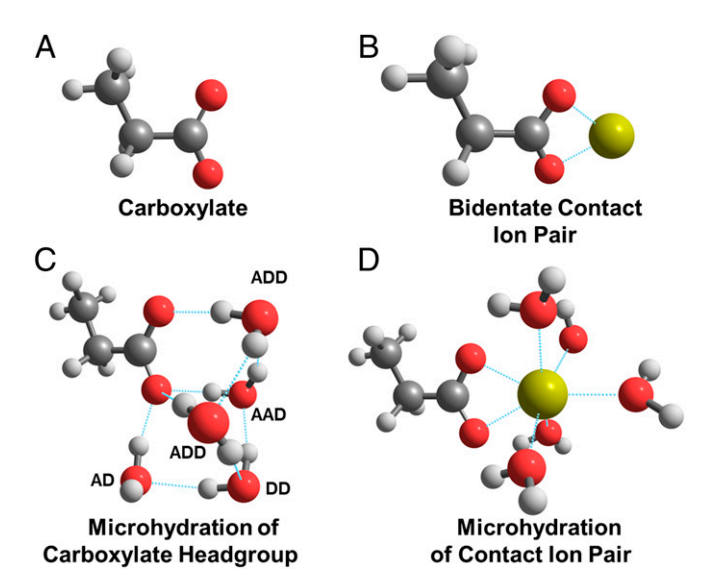


Fig. 2. Schematic structures illustrating the variations in binding motifs for the Ca^{2+} (B) and water molecules (C) to the carboxylate head group (A) as well as in the microhydration of the Ca^{2+} -RCO $_2^-$ contact ion pair (D). Hydrating waters are labeled according to their roles as hydrogen bond acceptors (A) and donors (D). Structures obtained at the MP2/aug-cc-pVDZ level (SI Appendix has details) are presented for (A) d-OPr $^-$ (B) d-[Ca $^{2+}$ -OPr $^-$] $^+$. (C) d-OPr $^-$ (H_2 O) $_5$, and (D) d-[Ca $^{2+}$ -OPr $^-$] $^+$. (H_2 O) $_5$. The Ca $^{2+}$ ion, when present, is indicated in yellow.

acid (d₃₅-SA) variation was used to ensure that the acid moiety remains anchored at the interface in the high-pH study.

The combination of mass spectrometry and optical spectroscopy methods used here has been described in detail previously (40), and it has been used to measure vibrational spectra of sizeselected ions using a double-focusing, tandem time-of-flight photofragmentation mass spectrometer. Briefly, ions are extracted from solution using electrospray ionization and accumulated in a variable temperature (10-100 K) radiofrequency ion trap before injection into the time-of-flight region. The spectra of the small clusters yield structural information about strongly bound water molecules in the first hydration shell and were, therefore, obtained using the mass "tagging" technique. In this approach, vibrational spectra of the cold ions are acquired in a linear action mode through photoevaporation of a weakly bound adduct (in this case, He, H₂, or D₂). For larger clusters, which were produced in decreasing abundance in the ion source, the spectra were obtained by monitoring the infrared multiple photon-induced dissociation (IRMPD) of a more weakly bound water molecule in the second hydration shell. The IRMPD spectra display broader peaks (Full width at half max is ~28 vs. 13 cm⁻¹ for bare and D₂-tagged d-[Ca²⁺·OPr⁻]⁺·(H₂O)₅, respectively) as expected for the warmer clusters sampled by this technique. The resulting band maxima, however, are very similar for the 2 methods (within 7 cm⁻¹), and the observed bands are found to be insensitive to temperature from 20 to 100 K as shown in SI Appendix, Fig. S2.

Vibrational spectra of size-selected d-OPr⁻ (H₂O)_n clusters over the range n=0 to 14 are presented in Fig. 3 A-I along with the IRRAS spectrum of d_{35} -SA on D_2 O at pD = 10.5 (Fig. 3I; reproduced from Fig. 1B) with the observed ν_s^{COO} and ν_{as}^{COO} frequencies listed in SI Appendix, Table S2. Note that the ν_{as}^{COO} band in the n=14 spectrum is very close to that of d_{35} -SA at the air–water interface (1,549 vs. 1,553 cm⁻¹, respectively), indicating that the local interactions around the head group are sufficiently developed in this size regime to recover macroscopic behavior. In contrast to the trend previously reported for the d-[Mg²⁺·OPr⁻]⁺ complex (36), the ν_{as}^{COO} features in the d-OPr⁻ (H₂O)_n clusters exhibit a normal solvatochromic red shift, while it is now the ν_s^{COO} bands that exhibit the unusual blue shift with increasing hydration. As such, the ν_s^{COO} and ν_{as}^{COO} bands in d-OPr⁻ (H₂O)_n converge toward each other as they approach their respective bulk limits from opposite directions.

On closer inspection of the progression presented in Fig. 3, the CO bands do not evolve smoothly in the n = 5 to 7 range, where we expect the completion of the first hydration shell around the anionic head group (42–44). The n = 5 spectrum is particularly interesting, as the incremental band shift breaks with the prevailing trend by becoming more widely split before the convergent evolution continues above n = 6. These features can be understood in the context of minimum energy structures recovered from electronic structure calculations, with the detailed geometries presented in SI Appendix, Fig. S3. These structures largely follow those reported by Marcum and Weber (45) and Motegi et al. (46) for the $CH_3NO_2^-(H_2O)_n$ clusters. An exception, however, is the n = 5 arrangement that is calculated to exhibit the observed discontinuity in the splitting between the 2 CO stretching bands. Two low-lying n = 5 structures and their corresponding vibrational spectra are included in Fig. 4 to illustrate how the local solvation network drives the splitting between the bands. The main difference between the 2 arrangements is that they have different numbers of H-bond donors to the 2 oxygen atoms on the anion. Only the structure in Fig. 4B reproduces the experimental splitting (211 vs. 214 cm⁻¹ for calculated [Fig. 4D] and observed [Fig. 4E], respectively). The water network in Fig. 4B adopts an arrangement in which 3 H bonds are donated to one of the O atoms on the anionic head group, while the other O atom only has one (hence denoted $5_{3:1}$).

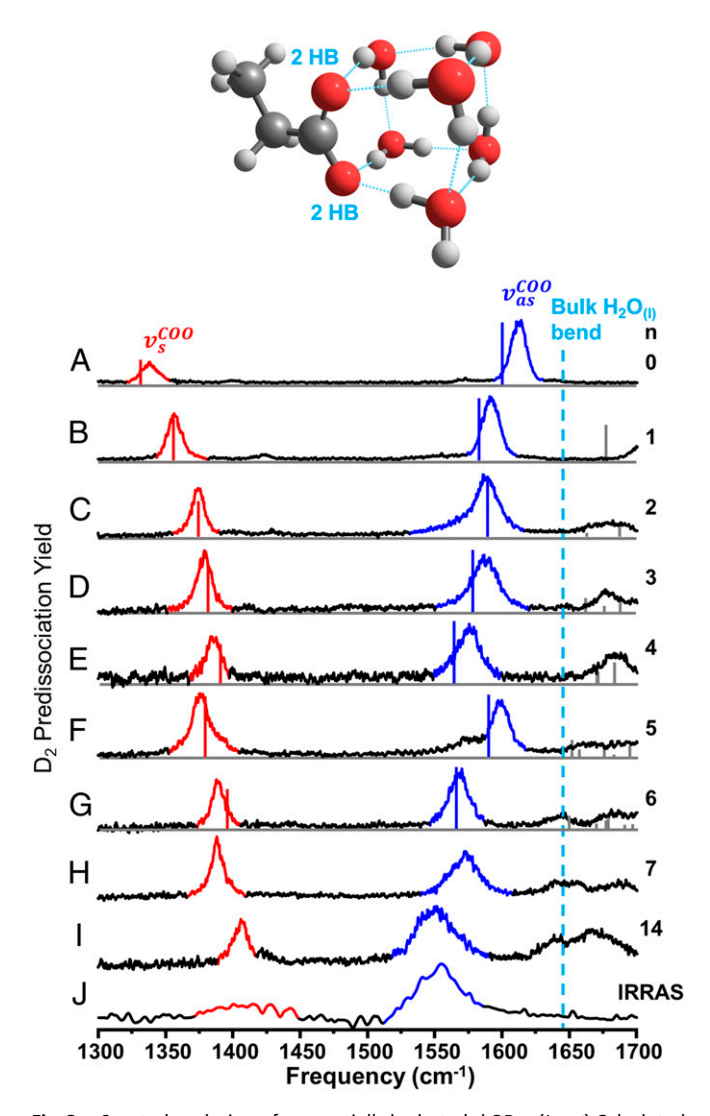


Fig. 3. Spectral evolution of sequentially hydrated d-OPr $^-$. (Inset) Calculated (MP2/aug-cc-pVDZ) minimum energy structure of d-OPr $^-$.(H_2O)₆. The number of H-bond donors to each oxygen on the anion is labeled HB. (A-I) Vibrational predissociation spectra of d-OPr $^-$.(H_2O) $_{n=0 \text{ to } 7, 14}$ ·D $_2$. Peaks assigned to ν_s^{COO} and ν_{as}^{COO} are colored red and dark blue, respectively. A-G also contain vibrational stick spectra calculated at the MP2/aug-cc-pVDZ level of theory (frequencies scaled by 0.986) for the corresponding minimum energy cluster geometries (included in SI Appendix, Fig. S3). (J) The IRRAS spectrum of a d_{35} -SA monolayer (20.5 Å 2 per molecule) with a subphase pD of 10.5 reproduced from Fig. 1B is inverted here for clarity. The light blue line at the right denotes the position of the H_2O bend in bulk water (41).

The other isomer, shown in Fig. 4*A*, is calculated to follow the overall trend in CO band evolution (i.e., with a smaller [163-cm⁻¹] splitting [Fig. 4*C*]) and has a more symmetrical arrangement in which 2 H bonds are donated to each O atom (denoted 5_{2:2}). The 5_{3:1} structure is calculated to be lowest in energy, lying 200 cm⁻¹ below the 5_{2:2} structure at the MP2/aug-cc-pVdZ level when including the counterpoise correction for basis set superposition error (47) and vibrational zero-point contributions. Thus, the directional nature of the H bonds to the nearby water molecules has a significant impact on the head group response.

We next turn to the spectral evolution of the d- $[Ca^{2+} \cdot OPr^{-}]^{+} \cdot (H_2O)_{n=0 \text{ to } 12}$ clusters, which is presented in Fig. 5 B-J with the ν_s^{COO} and ν_{as}^{COO} frequencies listed in SI Appendix, Table S3. The d-OPr $^-$ spectrum (Fig. 5A) and IRRAS spectrum of d_{31} -palmitic acid $(d_{31}$ -PA) on a 0.3 M $CaCl_{2(aq)}$ subphase in Fig. 5K are

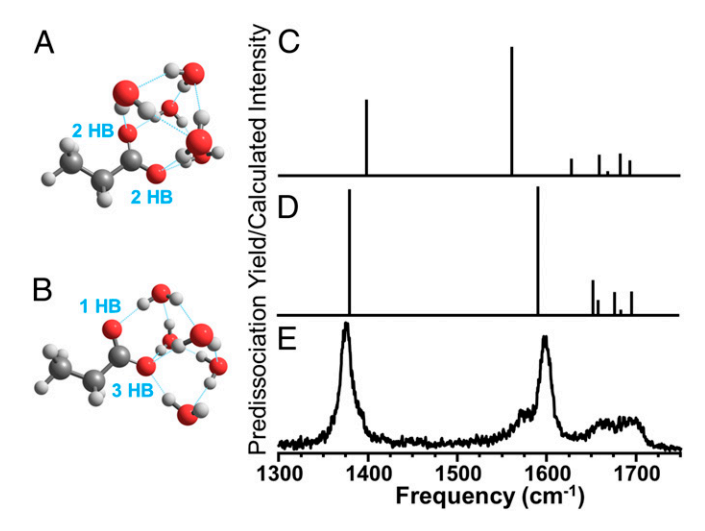


Fig. 4. Comparison of the lowest-energy isomers of d-OPr $^-$ (H₂O)₅. In A and B, calculated (MP2/aug-cc-pVDZ) structures of (A) $5_{2:2}$ and (B) $5_{3:1}$ with their respective spectra displayed in C and D, respectively (after scaling the calculated frequencies by 0.986), are shown along with the experimental spectrum of d-OPr $^-$ (H₂O)₅-D₂ in E reproduced from Fig. 3F. The number of H-bond donors to each oxygen on the anion is labeled HB.

reproduced from Figs. 1C and 3A, respectively. As was the case in the d-[Mg²⁺·OPr⁻]⁺·(H₂O)_{n=0 to 4} series (36), the ν_{as}^{COO} band is most responsive to hydration (as well as to metal complexation) and exhibits a blue shift as it approaches the interfacial limit. The ν_{s}^{COO} band displays a much more modest solvatochromic red shift, approaching the 1,435-cm⁻¹ value observed by SFG (12) at n = 12 (1,448 cm⁻¹). (Note that the ν_{s}^{COO} band is much more evident in the SFG spectrum due to the different selection rules for IRRAS vs. SFG [48, 49].) The ν_{as}^{COO} band is quite close to the interfacial limit by n = 12, again indicating that the local mechanics driving the shifts are largely converged on completion of the second solvation shell. We remark that the interfacial band displays a doublet structure, contributing to the broader width of this feature.

The most important aspect of the d-[Ca²⁺·OPr⁻]⁺·(H₂O)_{n=0 to 12} spectra is that the key ν_{as}^{COO} feature (dark blue in Fig. 5) at n = 12 appears very close to that displayed by the interface while still in a regime where the metal ion is necessarily in close contact with the head group. From n = 1 to n = 5, which corresponds to the completion of the first hydration shell (50–54), the calculated structures feature the cation docked in a bidentate motif to the head group and all of the H₂O molecules directly attached to the cation as seen in *SI Appendix*, Fig. S4. This arrangement is predicted to yield vibrational fundamentals (dark blue and red stick spectra in Fig. 5 A-G) in good agreement with the observed trend. Note that the water bending mode exhibits a red shift on completion of the first hydration shell but then, blue shifts toward the bulk value (dashed line in Fig. 5) (41) as subsequent water molecules overwhelm the contribution from those tightly held in the interior by n = 12.

To address the possible role of different local binding motifs in the contact ion pair as well as solvent-separated configurations of the system, constant number, volume, and temperature (NVT) ab initio molecular dynamics (AIMD) simulations were carried out at the B3LYP+D3/6-31G(d) level of theory. The contact ion pair form of the n=10 cluster was maintained even when the simulations were run at T=300 K and for as long as 12 ps. These calculations indicate that the contact ion pair motif is retained as water molecules are added in the second solvation shell. As such, because the observed ν_{aso}^{COO} band is quite close to that of the interfacial asymptote by n=12, we conclude that this feature

may be generated by hydration of the contact ion pair. The range of CO stretching frequencies at play in the various isomers available to the n=6, 8, and 10 hydrates is presented in *SI Appendix*, Fig. S5 to explore how different hydration motifs that are likely adopted at high temperature affect the spectrum. *SI Appendix*, Fig. S6 and Table S4 presents the positions of calculated spectral transitions and structures for several isomers of d-[Ca²⁺·OPr]+·(H₂O)_{n=6, 8, 10}. This exercise accounts for about half of the breadth (~50 cm⁻¹) observed for the ν_{as}^{COO} bands at the interface. Bulk aqueous-phase AIMD simulations of the acetate ion response to proximal Ca²⁺ ions are included in *SI Appendix*, Fig. S7, which further illustrates the spectral responses of various binding configurations.

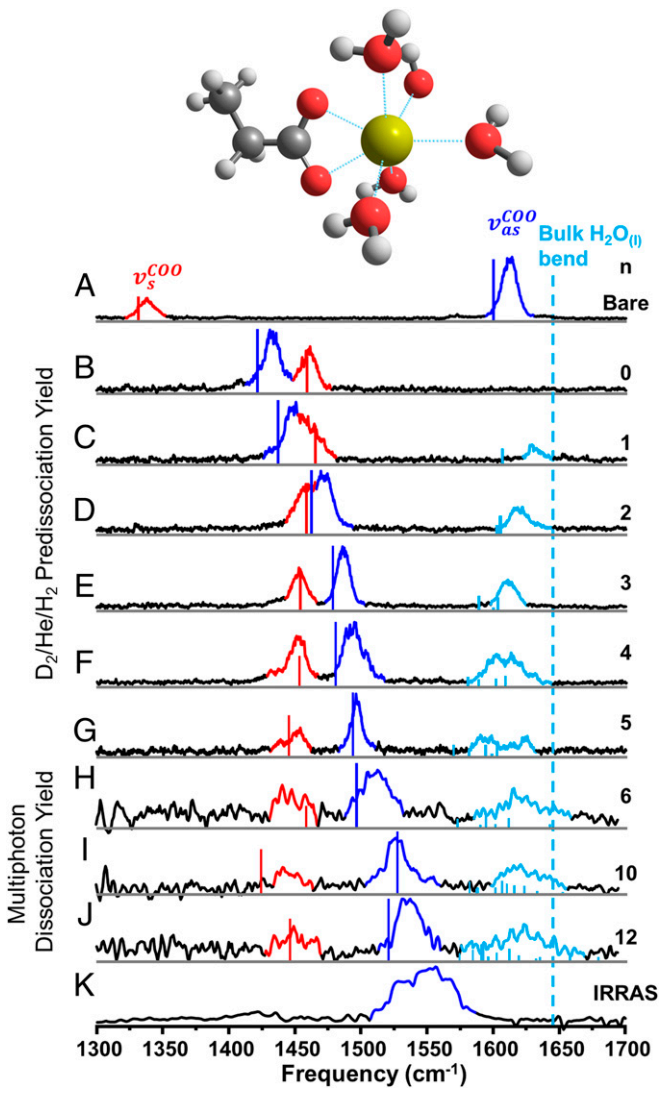


Fig. 5. Spectral evolution of sequentially hydrated d-[Ca²⁺·OPr⁻]+. (*Inset*) Calculated MP2/aug-cc-pVDZ minimum energy structure of d-[Ca²⁺·OPr⁻]+. (H_2O)₅. Gas-phase cluster spectra for (A) d-OPr⁻D₂, (B-G) d-[Ca²⁺·OPr⁻]+.(H_2O)_{n=0 to 5}·X (X = He for n = 0, H₂ for n = 1–5), and (H-J) IRMPD spectra of d-[Ca²⁺·OPr⁻]+.(H_2O)_{n=6}, 10, 12. A-J also contain vibrational stick spectra for the corresponding minimum energy cluster geometries (*SI Appendix*, Fig. S4) calculated at the MP2/aug-cc-pVDZ level of theory (scaled by 0.986). Peaks assigned to v_s^{COO} , v_{as}^{COO} , and the water bend are colored red, dark blue, and light blue, respectively. The light blue line denotes the position of the H₂O bend in bulk water (41). (K) Inverted IRRAS spectrum of d_{31} -PA monolayer (20.5 Å² per molecule) on 0.3 M CaCl₂, reproduced from Fig. 1C. B is adapted with permission from ref. 36. Copyright 2017 American Chemical Society.

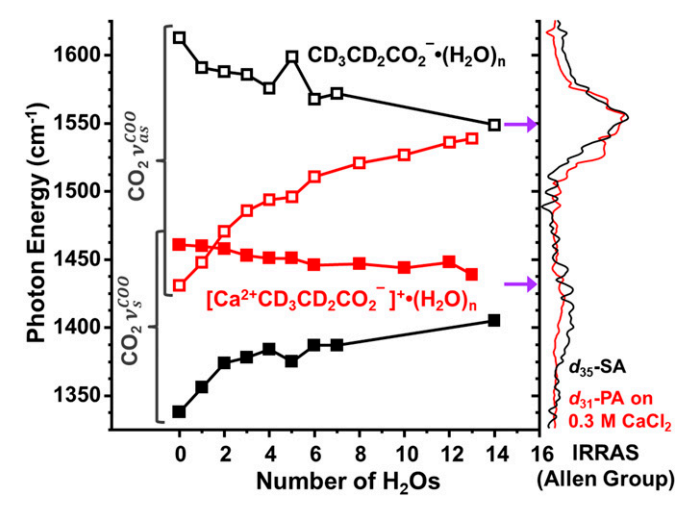


Fig. 6. Overview of the spectral evolution of d-OPr $^-$ (H₂O)₀ and d-[Ca²⁺·OPr $^-$]+· $(H_2O)_n$ bands toward interfacial positions. (Left) The energies of the ν_s^{COO} and $\nu_{\rm as}^{\rm COO}$ transitions for sequentially hydrated gas-phase clusters are denoted by solid and hollow boxes, respectively. The black traces correspond to d-OPr- $(H_2O)_{n_1}$ and the red traces correspond to d- $[Ca^{2+}\cdot OPr^-]^+\cdot (H_2O)_{n_2}$. (Right) The IRRAS spectra for 20.5 Å^2 per molecule d_{35} -SA and 20.5 Å^2 per molecule d_{31} -PA on 0.3 M CaCl₂ are plotted as black and red lines, respectively. Purple arrows denote the locations of $\nu_{\rm s}^{\rm COO}$ and $\nu_{\rm as}^{\rm COO}$ in lithium phenylacetate (55).

Fig. 6 presents a summary of the band evolutions in the clusters for the bare carboxylate (Fig. 6, black) and the contact ion pair (Fig. 6, red) along with the bulk asymptotes reproduced from Fig. 1. This presentation emphasizes important observations from this study: 1) both systems closely approach the behavior of the bulk interface in the size range corresponding to filling the second hydration shell, 2) the 2 CO stretching features approach these asymptotes with opposite solvatochromic shifts, and 3) the shifts in the contact ion pair are opposite from those displayed by the bare ion.

We next address the interactions that underlie these trends. We note that the ν_{as}^{COO} band is most directly responsive to the force constants describing the CO₂ moiety, while the situation regarding the ν_s^{COO} mode is complicated by strong mixing with the C-C stretching mode mentioned above. In our earlier study (36), we pointed out that the behavior of the ν_{as}^{COO} band could be understood in a scenario where the direct attachment of the divalent metal ion to the head group yields a large electric field. This effectively polarizes the carboxylate scaffold to both shorten the C-C bond and weaken the C-O bonds as electron density is drawn into the antibonding molecular orbitals of the -CO₂⁻ group (56). This rationalizes the extreme red shift of the $\nu_{nc}^{\tilde{COO}}$ band from the isolated carboxylate to the bare contact ion pair as well as the relaxation of this red shift as polarized water molecules add directly to the metal ion. The latter process effectively reduces the local electric field for all species in the primary hydration shell of the cation. More specifically, reduction of the electric field at the RCO₂ site diminishes the polarization-induced band shifts in the bare complex and incrementally drives the system back toward the unperturbed position of the free anion with increasing hydration. The overall trend in the d-[Ca²⁺OPr⁻]⁺ system is very similar to that found in the Mg2+ complexes, indicating that the spectral response is not strongly dependent on the metal ion radius.

We note that the electric field argument can also rationalize the solvatochromic shifts displayed by the d-OPr $^-$ ·(H₂O)_n system. In that case, the hydration of the head group will act to create a reaction field from the array of water molecules in its first hydration shell (57). This field lies in the same direction as that created by direct contact with a cation. Since the cationic response is to red shift the ν_{as}^{COO} transition but blue shift that due to ν_s^{COO} , it is apparent that the water network's hydrogens (with their δ^+ charges) perform a similar role as the Ca²⁺ charge. Although water cannot create a projected electric field as strong as that from the divalent ion, it is interesting to note that fully hydrated d-OPr yields CO bands very close to those displayed by the isolated lithium phenylacetate contact ion pair (purple arrows on the right in Fig. 6). As such, the net effect of hydration seems to be quantitatively equivalent to that obtained from a single positive charge.

To gain a more quantitative estimation of how local electric fields evolve around the charge centers on hydration, we calculated the magnitude of the projected electric field along the C–C bond (evaluated at the central carboxylic C atom) for the minimum energy structures of both d-OPr⁻ and d-[Ca²⁺·OPr⁻]⁺ systems as a function of hydration number. Here, we neglect the internal fields coming from the vibrational chromophore itself and only consider the point charge field sources outside it. These results are collected in SI Appendix, Fig. S8 for all bond projections of the field. We find that only the electric field projected along the C-C bond is strongly correlated with the observed band shifts as displayed in Fig. 7, which compares the observed ν_{as}^{COO} energies of the d-OPr $^-$ (H₂O) $_{n=0 \text{ to } 6}$ anions (\blacksquare in Fig. 7) and d-[Ca²⁺·OPr⁻]⁺·(H₂O)_{n=0 to 6} cations (\blacktriangle in Fig. 7) with the electric field components along the C-C bond axis.

Finally, it is useful to consider the spectroscopic behavior of the CO stretching frequencies of the RCO₂ group in the context of widely used theoretical treatments to model the spectra of liquids. For example, in the case of pure water, the local electric field along the OH groups is typically regarded as the most important factor driving the local OH stretching fundamentals (58-60), whereas our results on the carboxylate group indicate that fields along the CO bonds are not strongly correlated with CO spectral shifts. Because of the different couplings in H₂O, the symmetric and asymmetric stretch splittings observed for H₂O are much smaller than the condensed-phase broadening due to thermal effects and hydrogen bonding. Thus, the field projected onto a single OH oscillator is sufficient to describe the condensedphase spectra (58–60). For the solvation of the RCO₂⁻ group considered herein, the splittings between the symmetric and asymmetric CO stretch vibrations are large compared with the shifts of the CO oscillators that arise from the thermal broadening in the condensed-phase environment. It is more likely that the RCO₂ group response is a result of (at minimum) 3-fold

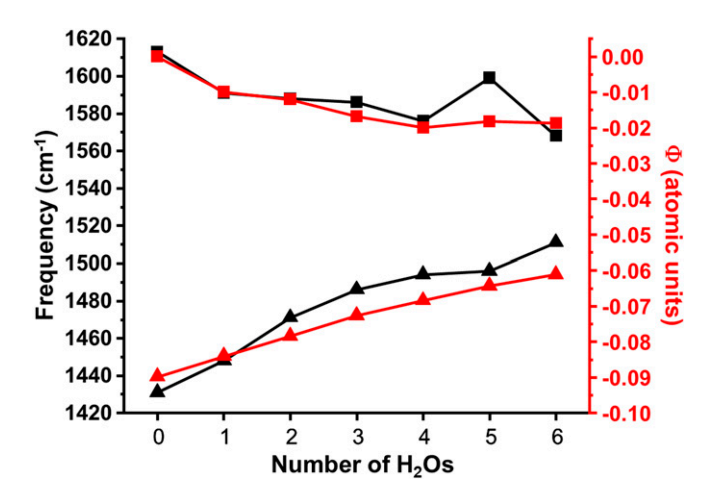


Fig. 7. The observed frequencies of the ν_{as}^{COO} fundamentals in d-OPr $^-$ (H₂O)_{n=0 to 6} and d-[Ca²⁺·OPr⁻]⁺·(H₂O)_{n=0 to 6} are denoted by black squares and triangles, respectively. The magnitudes of the electric fields Φ (a.u.) along the C–C axis of d-OPr $^-$ (H₂O)_{n=0 to 6 and d-[Ca²⁺·OPr $^-$]+·(H₂O)_{n=0 to 6 are denoted by red}} squares and triangles, respectively.

mode coupling among the 2 CO groups and the C–C oscillator involving the central carboxylic C atom. As such, the behavior of the 3 transitions arising from the 3×3 coupling matrix should be taken as a signature of ion binding. This suggests that identification of the latter (C–C stretching) coupling activity in the spectrum should be a useful direction for additional work. In particular, it does not seem useful to regard the splitting between the bands commonly denoted as symmetric and asymmetric CO stretches to be a consequence of the coupling between local CO oscillators, a perspective often taken in the reconstruction of collective normal modes in simple triatomic systems (61).

Summary

We have reported how the features normally attributed to the CO stretching bands (ν_s^{COO} and ν_{as}^{COO}) in a carboxylate head group, both free and complexed with a Ca²⁺ ion, evolve from the bare ions to the features observed at the air—water interface with stepwise hydration. The band evolutions are observed to be complex such that the directions of solvatochromic shifts are strongly dependent on the nature of the ionic species. Theoretical analysis of these effects suggests a picture where the head group exhibits a structural response to the net local projected electric field along the C–C bond. As such, one cannot associate a particular splitting in a complex environment to the proximity of cations alone. The solvent plays a critical role as well such that the factors—solvent and charge—act in concert to drive the CO stretching band response. The spectra of fatty acids at the air—

statements about the local structures of ions at the charged airwater interface. In this regard, it would be especially useful to extend these studies to include systems that display a clear dependence of the CO stretching bands on metal ion presence that falls well outside the intrinsic solvatochromic response of the bare RCO₂⁻ anions.

ACKNOWLEDGMENTS. M.A.J. and H.C.A. thank the NSF through NSF Center for Aerosol Impacts on Chemistry of the Environment Grant CHE-1801971 for supporting this work. M.A.J. thanks the Air Force Office of Scientific Research for funding the cryogenic spectrometer used in the gas-phase experiments under Defense University Research Instrumentation Program (DURIP) Grant FA9550-17-1-0267. M.D.B. was supported by the US Department of Energy, Office of Basic Energy Sciences, Biomolecular Materials Program at Pacific Northwest National Laboratory (PNNL); PNNL is operated by Battelle Memorial Institute for the US Department of Energy under Contract

DE-AC05-76RL01830. S.M.K. and C.J.M. are supported by the US Department

of Energy, Office of Science, Office of Basic Energy Sciences, Division of

Chemical Sciences, Geosciences & Biosciences. K.D.J. is funded by Department of Energy Grant DE-FG02-00ER15066 and thanks the Center for Re-

search Computing, University of Pittsburgh, for computational resources.

This research used resources of the National Energy Research Scientific Com-

puting Center, a US Department of Energy Office of Science User Facility

operated under Contract DE-AC02-05CH11231.

water interface provide an excellent platform to disentangle these

competing effects. In particular, this approach reveals how the

contact ion pair and the bare carboxylate can yield surprisingly

similar spectroscopic signatures for the CO bands at the depro-

tonated head group. This work also underscores the potential

pitfalls of using these bands when attempting to provide definitive

- R. E. Cochran, T. Jayarathne, E. A. Stone, V. H. Grassian, Selectivity across the interface: A test of surface activity in the composition of organic-enriched aerosols from bubble bursting. J. Phys. Chem. Lett. 7, 1692–1696 (2016).
- R. E. Cochran et al., Analysis of organic anionic surfactants in fine and coarse fractions
 of freshly emitted sea spray aerosol. Environ. Sci. Technol. 50, 2477–2486 (2016).
- M. Mochida, Y. Kitamori, K. Kawamura, Y. Nojiri, K. Suzuki, Fatty acids in the marine atmosphere: Factors governing their concentrations and evaluation of organic films on sea-salt particles. J. Geophys. Res. 107, 4325 (2002).
- S. Li, L. Du, N. T. Tsona, W. Wang, The interaction of trace heavy metal with lipid monolayer in the sea surface microlayer. *Chemosphere* 196, 323–330 (2018).
- P. B. Petersen, R. J. Saykally, Probing the interfacial structure of aqueous electrolytes with femtosecond second harmonic generation spectroscopy. J. Phys. Chem. B 110, 14060–14073 (2006).
- D. E. Otten, P. B. Petersen, R. J. Saykally, Observation of nitrate ions at the air/water interface by UV-second harmonic generation. Chem. Phys. Lett. 449, 261–265 (2007).
- K. B. Eisenthal, Liquid interfaces probed by second-harmonic and sum-frequency spectroscopy. Chem. Rev. 96, 1343–1360 (1996).
- S. G. Grubb, M. W. Kim, T. Rasing, Y. R. Shen, Orientation of molecular monolayers at the liquid-liquid interface as studied by optical 2nd harmonic-generation. *Langmuir* 4, 452-454 (1988)
- E. M. Adams et al., Sodium-carboxylate contact ion pair formation induces stabilization of palmitic acid monolayers at high pH. Phys. Chem. Chem. Phys. 19, 10481–10490 (2017).
- E. M. Adams et al., Surface organization of a DPPC monolayer on concentrated SrCl₂ and ZnCl₂ solutions. Phys. Chem. Chem. Phys. 18, 32345–32357 (2016).
- C. Y. Tang, Z. Huang, H. C. Allen, Interfacial water structure and effects of Mg²⁺ and Ca²⁺ binding to the COOH headgroup of a palmitic acid monolayer studied by sum frequency spectroscopy. *J. Phys. Chem. B* 115, 34–40 (2011).
- C. Y. Tang, Z. Huang, H. C. Allen, Binding of Mg⁽²⁺⁾ and Ca⁽²⁺⁾ to palmitic acid and deprotonation of the COOH headgroup studied by vibrational sum frequency generation spectroscopy. *J. Phys. Chem. B* 114, 17068–17076 (2010).
- E. M. Adams, H. C. Allen, Palmitic acid on salt subphases and in mixed monolayers of cerebrosides: Application to atmospheric aerosol chemistry. *Atmosphere* 4, 315–336 (2013).
- M. C. K. Soule, P. G. Blower, G. L. Richmond, Effects of atmospherically important solvated ions on organic acid adsorption at the surface of aqueous solutions. J. Phys. Chem. B 111, 13703–13713 (2007).
- P. G. Blower, E. Shamay, L. Kringle, S. T. Ota, G. L. Richmond, Surface behavior of malonic acid adsorption at the air/water interface. *J. Phys. Chem. A* 117, 2529–2542 (2013).
- M. J. Shultz, C. Schnitzer, D. Simonelli, S. Baldelli, Sum frequency generation spectroscopy of the aqueous interface: Ionic and soluble molecular solutions. *Int. Rev. Phys. Chem.* 19, 123–153 (2000).
- P. B. Miranda, Q. Du, Y. R. Shen, Interaction of water with a fatty acid Langmuir film. Chem. Phys. Lett. 286, 1–8 (1998).
- A. P. Ault et al., Raman microspectroscopy and vibrational sum frequency generation spectroscopy as probes of the bulk and surface compositions of size-resolved sea spray aerosol particles. Phys. Chem. Chem. Phys. 15, 6206–6214 (2013).

- E. Le Calvez, D. Blaudez, T. Buffeteau, B. Desbat, Effect of cations on the dissociation of arachidic acid monolayers on water studied by polarization-modulated infrared reflection-absorption spectroscopy. *Langmuir* 17, 670–674 (2001).
- T. Zhang et al., Effect of pH and salt on surface pK_a of phosphatidic acid monolayers. Langmuir 34, 530–539 (2018).
- A. Gericke, H. Huhnerfuss, The effect of cations on the order of saturated fatty-acid monolayers at the air-water-interface as determined by infrared reflectionabsorption spectrometry. *Thin Solid Films* 245, 74–82 (1994).
- A. Gericke, H. Huhnerfuss, In-situ investigation of saturated long-chain fatty-acids at the air-water-interface by external infrared reflection-absorption spectrometry. J. Phys. Chem. 97, 12899–12908 (1993).
- J. E. Tackett, FT-IR characterization of metal acetates in aqueous solution. Appl. Spectrosc. 43, 483–489 (1989).
- K. Nakamoto, Infrared and Raman Spectra of Inorganic and Coordination Compounds (Wiley, New York, 1986).
- G. B. Deacon, R. J. Phillips, Relationships between the carbon-oxygen stretching frequencies of carboxylato complexes and the type of carboxylate coordination. Coord. Chem. Rev. 33, 227–250 (1980).
- C. C. R. Sutton, G. da Silva, G. V. Franks, Modeling the IR spectra of aqueous metal carboxylate complexes: Correlation between bonding geometry and stretching mode wavenumber shifts. Chemistry 21, 6801–6805 (2015).
- M. Nara, H. Torii, M. Tasumi, Correlation between the vibrational frequencies of the carboxylate group and the types of its coordination to a metal ion: An ab initio molecular orbital study. J. Phys. Chem. 100, 19812–19817 (1996).
- T. Dudev, C. Lim, The effect of metal binding on the characteristic infrared band intensities of ligands of biological interest. J. Mol. Struct. 1009, 83–88 (2012).
- M. Tafipolsky, R. Schmid, A consistent force field for the carboxylate group. J. Chem. Theory Comput. 5, 2822–2834 (2009).
- F. Quiles, A. Burneau, Infrared and Raman spectra of alkaline-earth and copper(II) acetates in aqueous solutions. Vib. Spectrosc. 16, 105–117 (1998).
- K. Nakamoto, Infrared Spectra of Inorganic and Coordination Compounds (Wiley, New York, 1963).
- S. Kundu, D. Langevin, Fatty acid monolayer dissociation and collapse: Effect of pH and cations. Colloids Surf. A Physicochem. Eng. Asp. 325, 81–85 (2008).
- A. W. Adamson, A. P. Gast, "Electrical aspects of surface chemistry" in *Physical Chemistry of Surfaces* (Wiley-Interscience, New York, ed. 6, 1997), pp. 169–224.
- J. K. Denton et al., 2019 Molecular-level origin of the carboxylate head group response to divalent metal ion complexation at the air-water interface. UC San Diego Library Digital Collections. https://doi.org/10.6075/J0JQ0Z7C. Deposited 22 June 2019.
- 35. J. W. DePalma, P. J. Kelleher, L. C. Tavares, M. A. Johnson, 2017 Data from "Coordination-Dependent Spectroscopic Signatures of Divalent Metal Ion Binding to Carboxylate Head Groups: H₂- and He-Tagged Vibrational Spectra of M²⁺·RCO₂⁻ (M=Mg and Ca, R = -CD₃, -CD₂CD₃) complexes." UC San Diego Library Digital Collections. https://doi.org/10.6075/J0J964K2. Deposited 12 May 2017.
- 36. J. W. DePalma, P. J. Kelleher, L. C. Tavares, M. A. Johnson, Coordination-dependent spectroscopic signatures of divalent metal ion binding to carboxylate head groups: H₂- and He-tagged vibrational spectra of M²⁺·RCO₂⁻ (M = Mg and Ca, R = -CD₃, -CD₂CD₃) complexes. *J. Phys. Chem. Lett.* **8**, 484–488 (2017).

- 37. M. Kakihana, M. Kotaka, M. Okamoto, Vibrational analysis of acetate ion molecules and estimation of equilibrium-constants for their hydrogen isotopic exchange-reactions. J. Phys. Chem. 87, 2526-2535 (1983).
- 38. M. Kakihana, T. Nagumo, Assignment for the infrared-spectrum of solid sodium propionate from low-temperature measurements in combination with C-13 isotopic shifts. Z. Naturforsch. **42**, 477–484 (1987).
- 39. E. Spinner, Vibration spectra of some substituted acetate ions. J. Chem. Soc., 4217-4226 (1964).
- 40. A. B. Wolk, C. M. Leavitt, E. Garand, M. A. Johnson, Cryogenic ion chemistry and spectroscopy. Acc. Chem. Res. 47, 202-210 (2014).
- 41. J. E. Bertie, M. K. Ahmed, H. H. Eysel, Infrared intensities of liquids. 5. Optical and dielectric constants, integrated intensities, and dipole moment derivatives of H₂O and D₂O at 22°C. J. Phys. Chem. 93, 2210-2218 (1989).
- 42. W. L. Jorgensen, J. Gao, Monte-Carlo simulations of the hydration of ammonium and carboxylate ions. J. Phys. Chem. 90, 2174–2182 (1986).
- 43. G. D. Markham, C. L. Bock, C. W. Bock, Hydration of the carboxylate group: An ab initio molecular orbital study of acetate-water complexes. Struct. Chem. 8, 293-307 (1997).
- 44. I. D. Kuntz, Hydration of macromolecules. 3. Hydration of polypeptides. J. Am. Chem. Soc. 93, 514-516 (1971).
- 45. J. C. Marcum, J. M. Weber, Microhydration of nitromethane anions from both a solute and solvent perspective. J. Phys. Chem. A 114, 8933-8938 (2010).
- 46. H. Motegi, et al., Theoretical study on the excess electron binding mechanism in the $[CH_3NO_2\cdot(H_2O)_n]^-$ (n = 1-6) anion clusters. J. Phys. Chem. 114, 8939-8947 (2010).
- 47. S. F. Boys, F. Bernardi, The calculation of small molecular interactions by the differences of separate total energies. Some procedures with reduced errors. Mol. Phys. 19, 553-566 (1970).
- 48. Y. R. Shen, D. Kim, W. Sung, Sum-frequency vibrational spectroscopic studies of Langmuir monolayers. Curr. Appl. Phys. 13, 619-632 (2013).
- 49. R. Mendelsohn, J. W. Brauner, A. Gericke, External infrared reflection absorption spectrometry of monolayer films at the air-water interface. Annu. Rev. Phys. Chem. 46, 305-334 (1995).

- 50. M. F. Bush, R. J. Saykally, E. R. Williams, Hydration of the calcium dication: Direct evidence for second shell formation from infrared spectroscopy. ChemPhysChem 8, 2245-2253 (2007).
- 51. M. F. Bush et al., Hydration of alkaline earth metal dications: Effects of metal ion size determined using infrared action spectroscopy. J. Am. Chem. Soc. 131, 13270-13277 (2009).
- 52. M. Pavlov, P. E. M. Siegbahn, M. Sandstrom, Hydration of beryllium, magnesium, calcium, and zinc ions using density functional theory. J. Phys. Chem. A 102, 219-228 (1998)
- 53. J. L. Fulton, S. M. Heald, Y. S. Badyal, J. M. Simonson, Understanding the effects of concentration on the solvation structure of Ca^{2+} in aqueous solution. I. The perspective on local structure from EXAFS and XANES. J. Phys. Chem. A 107, 4688–4696
- 54. F. Xiang et al., Hydration effect on interaction mode between glutamic acid and Ca²⁺ and its biochemical implication: A theoretical exploration. New J. Chem. 30, 890-900 (2006)
- 55. S. Habka, V. Brenner, M. Mons, E. Gloaguen, Gas-phase spectroscopic signatures of carboxylate-Li⁺ contact ion pairs: New benchmarks for characterizing ion pairing in solution. J. Phys. Chem. Lett. 7, 1192-1197 (2016).
- 56. R. M. Badger, A relation between internuclear distances and bond force constants. J. Chem. Phys. 2, 128-131 (1934).
- 57. L. Onsager, Electric moments of molecules in liquids. J. Am. Chem. Soc. 58, 1486–1493 (1936).
- 58. C. J. Fecko, J. D. Eaves, J. J. Loparo, A. Tokmakoff, P. L. Geissler, Ultrafast hydrogenbond dynamics in the infrared spectroscopy of water. Science 301, 1698-1702 (2003).
- 59. S. A. Corcelli, J. L. Skinner, Infrared and Raman line shapes of dilute HOD in liquid H₂O and D_2O from 10 to 90 °C. J. Phys. Chem. A 109, 6154–6165 (2005).
- 60. P. L. Geissler, Water interfaces, solvation, and spectroscopy. Annu. Rev. Phys. Chem. 64, 317-337 (2013).
- 61. E. B. Wilson, J. C. Decius, P. C. Cross, Molecular Vibrations: The Theory of Infrared and Raman Vibrational Spectra (McGraw Hill, New York, 1955).